Author: Bormuth, R.
Title: Chasing cosmic tau neutrinos in the abyss
Issue Date: 2017-12-07

1 INTRODUCTION

> Good resolutions [..] are simply cheques that men draw on a bank where they have no account
>
> — Oscar Wild, The Picture of Dorian Gray

In this chapter the motivation for observing the Universe with neutrinos is laid out. This process is called neutrino astronomy and offers a new window to the Universe which complements the traditional branches of astronomy. A brief historic overview as well as the current status of neutrino astronomy are presented.

Neutrino astronomy is especially relevant to the understanding of the origin of cosmic rays. Therefore, this chapter first focuses on the status of cosmic ray astronomy. This is followed by an introduction to neutrino astronomy and its link to cosmic ray astronomy.

1.1 COSMIC RAYS

Cosmic rays are sub-atomic particles which traverse the universe. They originate in outer space and were first observed over 100 years ago. Cosmic rays are believed to be accellerated in some astrophysical sources. For these particle accelerators, neutrinos can offer unique insights into their creation and evolution in time.

Since the discovery of cosmic rays, despite numerous efforts, some fundamental questions remain unanswered. The list of open questions includes the origin, propagation through the Universe and the acceleration mechanism of cosmic rays. This section will focus on the history and current status of cosmic ray research.

A brief history

Before the notion of cosmic rays existed, Charles-Augustin Coulomb in 1785 observed that a charged metal sphere will gradually loose its charge in air. From this observation, he and other scientist concluded that the air is ionized. At that time, the ionization was believed to be caused by radioactive elements in the Earth crust.

If Earth's crust is the origin of the radiation it implies a gradual decrease of ionization in air with increasing distance from the crust. This prediction was tested by Victor Hess in the years of 1911-1913. After greatly improving the measurement accuracies, Hess undertook several balloon flights in order to validate this theory. He found the radiation levels to increase with the distance from Earth, thereby falsifying the Earth crust theory. From his observations he concluded that there was radiation penetrating the atmosphere from outer space [1], today this radiation is commonly referred to as cosmic rays. This conclusion was confirmed by Werner Kolhörster in 1913 [2].

Clay in 1927 and Milikan in 1932 each undertook sea voyages to measure the dependence of the cosmic ray flux on Earth's latitude. Both found the flux to depend on the latitude which led to the conclusion that cosmic rays are affected by the Earth's magnetic field and therefore mainly composed of charged particles. Following up on this, other experiments showed an abundance of cosmic rays in cardinal direction from the west, proving them to be mainly positively charged.

In the early days of particle physics, cosmic rays led to important scientific discoveries in the field. Before the invention of particle accelerators, cosmic rays were the only way to study interactions of highly energetic particles. The positron was discovered by Carl D. Anderson in 1933 by observing interactions of cosmic rays in a cloud chamber in the presence of a magnetic field [3]. The magnetic field allowed to distinguish positively and negatively charged particles. Anderson also discovered the muon in 1936 in a similar experimental setup. In a different experimental setup, cosmic rays allowed for the discovery of the pion by Ochialini et.al. [4]. Today, particle accelerators have not reached the energies attainable with cosmic rays but the low flux of cosmic rays makes groundbreaking particle physics observations unfeasible.

Matter composition of Cosmic Rays

Following the early observations of cosmic rays, it could be concluded that most cosmic rays are nuclei, with protons being most common amongst them. Measuring the mass of the particle impinging on Earth's atmosphere is non trivial, especially as the energy of the cosmic ray particles increase. The current data agree on the most prevalent particles but vary in the exact composition. To give an idea, one example, Bluemer et al. estimate the composition to be: protons 85 %, helium 12 % and 1 % of nuclei with atomic number $Z \geqslant 3$. The remainder of the cosmic rays is composed of other particles such as electrons [5].

Anti-particles make up for a small fraction of the observed cosmic rays. At present, the bulk of the observed anti-particles are anti-protons and positrons [5]. Some neutral particles reaching Earth from outer space are believed to be neutrons. A different sample of high energetic particles in the Universe is composed of photons which are commonly referred to as Gamma Rays.

Energy spectrum

The cosmic ray energy spectrum for different primary particles is shown in Fig. 1. The energy spectrum of cosmic rays spans roughly 12 orders of magnitude. It is described reasonably well by a power law

$$\frac{dN}{dE} \approx E^{-\gamma} \quad , \tag{1}$$

where E is the energy of the primary particle and γ the so-called spectral index.

The energy spectrum is only depicted down to energies of one GeV because below those energies the modulation of the cosmic rays due to irregular solar wind magnetic field fluctuations is such that the energy spectrum is not well defined [6]. At energies below 0.1 GeV most cosmic rays originate from the sun. These are not considered in this work.

The best fit to the all particle energy spectrum has different spectral indices for different energy ranges. The two points where the spectral index significantly changes are the so-called knee at $E \simeq 5 \times 10^6$ GeV and the ankle at $E \simeq 5 \times 10^9$ GeV. From the lowest energies up to the knee the spectral index is approximately $\gamma \simeq 2.7$. At energies above the knee the spectral index changes to $\gamma \simeq 3$. At the ankle, the spectrum flattens to the original $\gamma \simeq 2.7$ and then steepens again [7].

The changes in spectral index indicate a change in origin, propagation or composition of the cosmic rays. Multiple theories for the cause of spectral index change exist. Most commonly, the knee is attributed to either a limit in the acceleration capability of galactic cosmic ray sources or galactic cosmic rays having sufficient energy to leave the galaxy or both. Whereas, the ankle is attributed to either a transition in origin from galactic to extra-galactic cosmic rays or to interactions of cosmic rays with other particles [8]. The reasoning for these assumptions and the mechanisms involved are discussed in the following.

Origin and propagation

To date, no sources of cosmic rays have been observed, but the origin of cosmic rays can be categorized into two types: galactic or extra galactic origin. The two possibilities can be distinguished due to the way cosmic rays interact with the galactic magnetic field. The galactic magnetic field is composed of two parts with a regular and random field which have different strengths in the disc and the halo of the galaxy, respectively [10, 11]. In the halo, the total magnetic field is weaker than in the disk but due to its larger size the halo magnetic field dominates the deflection of cosmic rays. The typical halo magnetic field has a strength of 0.3 nT and a height of around 1.4 pc.

A charged particle interacting with a magnetic field will follow a curved trajectory described by the Larmor radius:

$$r_L = \frac{p}{qB} = 1.08 \times 10^{-6}\text{pc} \times \frac{p \times c/\text{GeV}}{ZB/0.1\,\text{nT}} \quad , \tag{2}$$

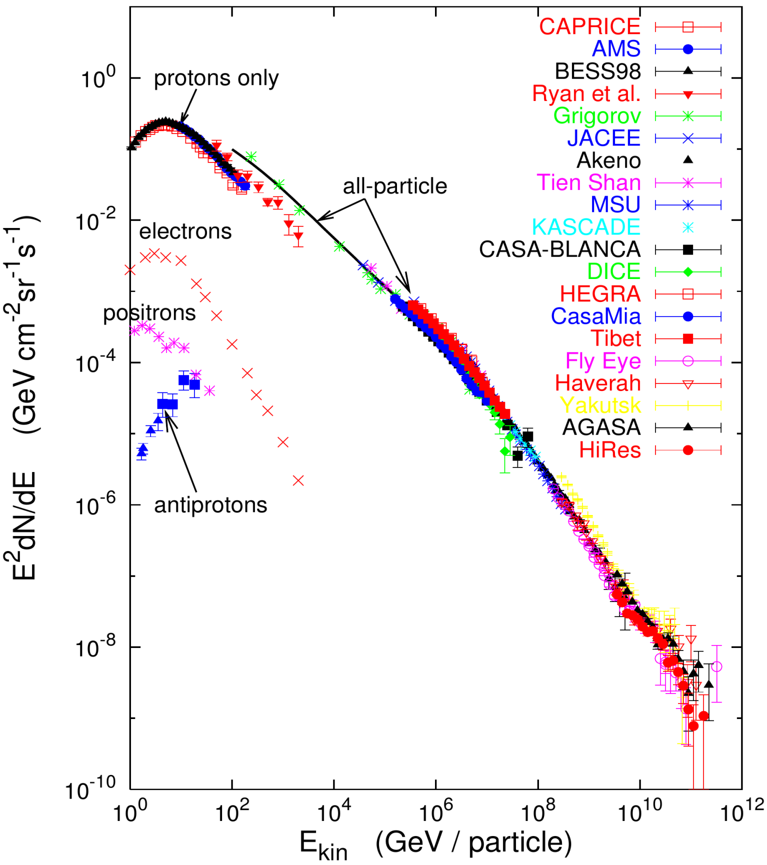

Figure 1: The energy spectrum of cosmic rays of different initial particles as measured by different experiments; The spectrum is reasonable well described by Eq. 1 with a varying spectral index γ, changing at the so-called knee ($E \simeq 5 \times 10^6$ GeV) and the ankle ($E \simeq 5 \times 10^9$ GeV); taken from [9].

where B is the magnetic field strength and p the particle momentum. For the typical halo magnetic field of 0.3 nT and a proton of energy 1×10^6 GeV the Larmor radius is 0.36 pc. A charged particle with a Larmor radius smaller than the galactic halo is confined to the galaxy. With energies above 1×10^9 GeV, the proton will leave the galaxy, making its detection at Earth less likely. Hence, cosmic rays with energies above the 1×10^9 GeV threshold are more likely to be of extra-galactic origin while cosmic rays of lower energies are assumed to be of galactic origin. This is one of the arguments associating the ankle in the cosmic ray energy distribution with a transition from cosmic rays of galactic to extra-galactic origin.

The discussed interaction of cosmic rays with the magnetic fields changes their direction and thereby making their origin untraceable. Only at the highest energies (around $E \simeq 1 \times 10^9$ GeV) the curvature of the particles is small enough so that the directions of the particles approximately point back to their origin. However, at these energies cosmic rays can interact with the cosmic microwave background (CMB) which causes them to lose energy. This effect is called the Greisen, Zatespin and Kuz'min cut-off [12] (GZK). It limits the distances cosmic rays can travel to around 200 Mpc. Protons with these energies can interact with the CMB via the Δ-resonance, causing the cosmic ray to lose energy (photo-disintegration) or produces a pion (pion-photo-production). Similarly, nuclei with these energies are also absorbed. As a result, the Universe becomes opaque to these cosmic rays. The interaction with the CMB produce photons and neutrinos at characteristic energies. Such photons and neutrinos have not yet been observed.

The energy threshold of the GZK cut-off is at the same energy as the ankle in the cosmic ray energy spectrum. Therefore, the drop-off at the ankle could also be explained by the GZK cut-off as cosmic rays of energies higher energies accumulate at lower energies.

The combination of the GZK cut-off and the galactic magnetic fields causes the identification of cosmic ray sources by the direct observations of cosmic rays to be unfeasible.

Cosmic Ray Sources

Identification of possible sources of cosmic rays is one of the main challenges of current research. In this section, a brief summary of the current knowledge is presented.

Source candidates for cosmic rays have to comply with the observed energy and intensity of the cosmic ray spectrum. It is generally agreed that the observed energies and fluxes can only be supplied by gravitational collapses of objects such as super nova remnants (SNR), often found in starburst galaxies, or by matter acreeting objects such as active galactic nuclei (AGN). These sources are discussed below.

A SNR is the structure remaining after the implosion of a star that produced the supernova. On the outskirts, a SNR is confined by an expanding shock

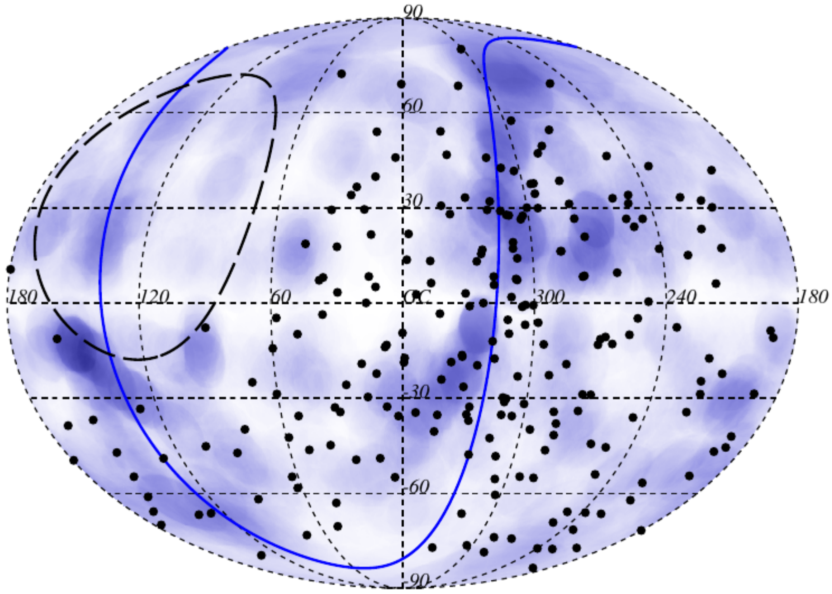

Figure 2: Skymap of the arrival directions (in galactic coordinates) of cosmic ray events with $E \geqslant 52\,\text{EeV}$ as detected by the Pierre Auger Observatory until the end of 2015 (black dots); the solid line depicts the field of view of the experiment for zenith angles smaller than $80°$; blue shapes represent the sources from the considered 2MRS catalog within a distance of $90\,\text{Mpc}$ which are in the field of view of the experiment; taken from [15].

wave. This shell consists of material ejected during the explosion and material picked up during its expansion from the interstellar matter. In the cosmic ray composition, a small relative abundance of iron atoms is recorded, which can be linked to the supernovae explosions of evolved early-type stars [6]. The shock waves can be an efficient particle accelerator (see a discussion below). Furthermore, supernovae and their implosions can produce the energy needed to support the intensity of the observed cosmic ray flux [13]. Recently, the Fermi collaboration reported the observation of the characteristic photon signal produced by the pion-photo-production effect for two SNRs (IC 443 and W 44) [14]. This detection is the first experimental evidence that correlates supernovae remnants with cosmic rays and is a strong indication that SNRs are sources of cosmic rays. Therefore, SNRs are the most likely explanation for the observed cosmic ray energy spectra and matter composition up to energies of $\mathcal{O}(1 \times 10^6\,\text{GeV})$. It is not expected that SNRs produce cosmic rays beyond this energy, due to their limited size and magnetic field strength.

Starburst galaxies are galaxies which undergo a phase of unusually high star production. The high star production rate is caused by a relative large amount of gas present in these galaxies. These are ideal conditions to form high-mass stars which are very bright and therefore likely to implode into supernovae. This makes starburst galaxies natural candidates for extra-galactic cosmic ray sources.

An AGN is a region of dense matter located at the center of a galaxy with a high luminosity in emitted photons. An early observation by the Pierre Auger Observatory in 2010 showed evidence for anisotropy in the arrival direction of cosmic rays correlated with the locations of AGNs [16, 17]. Due to their large size and the presence of strong magnetic fields, AGNs could be the sources of cosmic rays with energies in excess of $\mathcal{O}(1 \times 10^6\,\mathrm{GeV})$. An improved search on a larger data set in 2015 [15] could not reproduce this correlation for considered catalogs as shown in Fig. 2. If cosmic rays were still to originate from AGNs, limits on magnetic fields and cosmic ray fluxes from AGNs can be set [18].

Acceleration mechanism

The highest energies at which cosmic rays are observed at Earth are significantly higher than the temperature of the sources discussed before. Therefore, cosmic rays have to undergo further acceleration. A possible scenario for the acceleration is that the particles interact with moving magnetic fields. The mechanisms discussed here cover models for cosmic ray acceleration due to SNRs and AGNs.

The first mechanism for cosmic ray acceleration was proposed by Fermi in 1949 [19]. The mechanism involves the repeated scattering of charged particles on moving magnetic shock waves. Such shock waves exist in the Universe in form of magnetic gas clouds. A sketch of such a process is shown in Fig. 3a. Considering a particle moving at speed v with mass m scattering of a gas cloud moving at speed u, the energy gain per scattering is given by:

$$\Delta E_{\pm} = \frac{1}{2} m (v \pm u)^2 - \frac{1}{2} m v^2 \quad , \tag{3}$$

where the relative sign is linked to the alignment of the directions of v and u; if they are parallel it is positive, if they are anti parallel it is negative. In general, a particle will scatter multiple times, causing an energy gain per pair of parallel and anti-parallel scattering of $\Delta E = m u^2$ and an average energy gain of:

$$\frac{\Delta E}{E} = 2 \frac{u^2}{v^2} \quad . \tag{4}$$

Equation. 4 also holds for relativistic calculations [20]. This process is called 2^{nd} order Fermi acceleration due to the cloud velocity contributing quadratically in Eq. 4.

During the acceleration process, particles will also suffer energy losses due to interactions with the medium. For charged particles the most dominant energy loss is caused by synchrotron radiation and ionization. For a proton, the energy gain can become larger than the energy loss for energies greater than 200 MeV or so. The problem of particles achieving this initial energy is called the injection problem. It is currently not clear how particles achieve these initial energies.

The energy losses can explain the absence of electrons in the observed cosmic ray spectrum since they suffer more from radiation losses than heavier charged particles. For electrons at initial energies higher than 300 MeV or so, energy loss due to radiation outweighs the energy gain by acceleration.

The 2nd order Fermi acceleration processes can in principle be repeated an infinite amount of times. The energy is then only limited by the size of the accelerator and the strength of the magnetic field.

The acceleration process proposed by Fermi in 1949 was extended in the 1970's by different groups [21, 22]. This work focused on the impact of shock fronts created by super nova explosions on particle accelerations. In this process a particle will gain energy by passing over a shock front multiple times. In Fig. 3b such a process is sketched for a particle of speed v hitting a shock front moving at speed u_1. On both sides of the shock the particle can scatter off magnetic field irregularities which allows some particles to scatter from upstream to downstream multiple times. The gas behind the shock waves streams away from the shock front at a speed u_2 causing the gas to have a relative velocity of $u_1 - u_2$. The relative energy gain is then given by:

$$\frac{\Delta E}{E} = 2\frac{(u_1 - u_2)}{v} \quad . \tag{5}$$

A more sophisticated relativistic calculation taking into account different scattering angles as illustrated in [13] results in a similar linear dependence on the energy, namely:

$$\frac{\Delta E}{E} = \frac{4}{3}\frac{(u_1 - u_2)}{c} \quad . \tag{6}$$

Since this mechanism has a linear dependence on the velocity of the shock front it is commonly referred to as 1st order Fermi acceleration.

Both mechanisms result in a power law spectrum for the energy of the cosmic rays as observed in Eq. 1. Assuming a fixed escape probability, the power law nature of the spectrum is the result of combining the typical mean free path of a cosmic ray and the average energy gain per acceleration. In the case of the 1st order Fermi acceleration the two effects result in a spectral index of $\gamma = 2$ while for the 2nd order the spectral index cannot be uniquely determined [20].

It is generally believed that the two Fermi mechanisms together can accelerate particles starting from arbitrary initial energies to the highest energies observed for cosmic rays at Earth. Therefore, the injection problem of the 2nd order acceleration is overcome by accelerating particles to sufficient energies using the 1st order Fermi acceleration. However, evidence for this hypothesis has not yet been found.

Acceleration of cosmic ray in AGNs is believed to be a stochastic process connected to the 2nd order Fermi mechanism. Close to the center of an AGN highly turbulent magnetic fields can accelerate particles to energies above the injection problem. Once a particle reaches the injection energy, they scatter off time varying magnetic fields by means of the 2nd order Fermi mechanism. The existence of such fields was predicted in reference [23]. A calculation of this mechanism as performed in reference [24] shows that particles can be accelerated up to $\simeq 10 \times 10^{11}$ GeV within $\simeq 1 \times 10^{6}$ years in such environments.

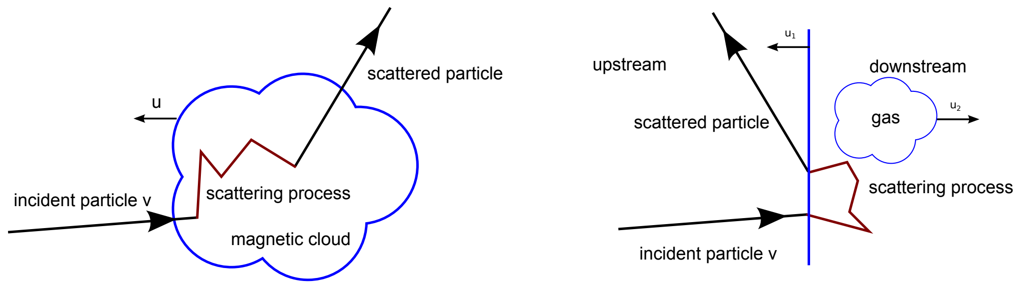

(a) 2^{nd} order Fermi: Acceleration of a charged particle of incident velocity v on a magnetic gas cloud.

(b) 1^{st} order Fermi: Acceleration of a charged particle of incident velocity v on a shock front moving with velocity u_1.

Figure 3: Sketches of the two Fermi acceleration mechanisms (see text).

The spectral index can be reproduced depending on the assumed magnetic fields in these sources. The cut-off in the energy distribution of cosmic rays can thus be caused either due to an exhaustion of the source power or the GZK cut-off.

1.2 NEUTRINO ASTRONOMY

Neutrino astronomy is a branch of astronomy utilizing very large neutrino detectors. The neutrino's small cross section and zero charge allows them to escape dense areas and travel through the Universe without being deflected or absorbed. These unique characteristics enable unprecedented observation opportunities, most notably the identification of the sources of cosmic rays. If cosmic rays interact within the vicinity of their source, pions will be produced which inevitable decay into neutrinos. Detection of these neutrinos will reveal the origin of the cosmic rays.

In this chapter the properties of neutrinos important for neutrino astronomy are discussed followed by an introduction to the concepts of neutrino astronomy.

1.2.1 *Neutrino history and properties*

The existence of the neutrino was postulated by Wolfgang Pauli in 1930 [25] to explain the observed energy spectrum of the electron in radioactive decays of atomic nuclei. The first direct detection was achieved following a proposal by Ganchang in 1942 [26] by Cowan and Reines in 1956 [27]. The experiment was based on the capture of anti-electron neutrinos produced in a nuclear reactor.

In 1962, following the discovery of the muon and the development of a pion beam, Lederman, Schwartz and Steinberger made the first direct detection of the muon neutrino [28]. The existence of the tau neutrino was postulated as a result of the development of the Standard Model of particle physics and the discovery of the tau lepton. Direct detection of the tau neutrino was first achieved by the DONUT experiment in 2001 [29]. Also with the development of the Standard Model, the force which describes neutrino interactions was unified with the electro-magnetic force. This force is called the weak interaction.

The weak interaction was found to be parity violating in a series of experiments in the years of 1956-58 [30]. This is formulated in the Standard Model as the left-handedness of neutrinos and the right-handedness of anti-neutrinos. To this day, no right-handed neutrino or left-handed anti-neutrino has been observed, suggesting they do not exist.

The Homestake experiment in 1962 [31] was the first in a series of experiments to detect neutrinos produced by the sun. The observed lack of solar neutrinos led to the discovery neutrino flavor oscillations (for more information see Section 1.2.1.1).

This discovery implied that neutrinos are massive particles. The current best global fit to all measurements can be found in reference [32]. Because two mass differences are measured via neutrino oscillations, the ordering of mass eigenstates is limited to two scenarios: referred to as the normal hierarchy ($m_{\nu_1} < m_{\nu_2} < m_{\nu_3}$, NH) and the inverted hierarchy ($m_{\nu_3} < m_{\nu_1} < m_{\nu_2}$, IH).

1.2.1.1 *Neutrino oscillations*

As discussed previously neutrinos change their flavors while travelling through space. This phenomenon is called neutrino oscillations. It is in analogy with the mixing between mass and weak eigenstates in the quark sector as described by the so-called CKM mixing matrix [33].

The first experimental evidence for neutrino oscillations was found by Ray Davis in the 1960s in the Homestake experiment [31]. A deficit of the predicted solar neutrino flux was found. This finding was originally called the solar neutrino problem and was only later understood as a consequence of neutrino oscillations. First proposed solutions to the solar neutrino problem suggested errors in the solar model. Doubts on the solar neutrino models were rebut by other experiments thereby confirming the solar model [34, 35]. Further progress in helioseismology and more precise measurements proved the solar model to be accurate.

One way of solving the solar neutrino problem is for the neutrinos to have mass allowing the mass eigenstates of the neutrinos to mix with the flavor eigenstates, giving rise to neutrino oscillations. The possibility of this mechanism was first proposed by Bruno Pontecorvo in 1957. After the discovery of the solar neutrino problem, Pontecorvo and Gribov utilized this mechanism to explain the observed deficit [36]. They proposed that the deficit in the observed electron neutrino rate was caused by oscillations of electron neutrinos into other flavors, which were not detected by the experiments.

Neutrino oscillations can be described by a unitary matrix which translates flavor and mass eigenstates into each other as shown in Eq. 7 and 8:

$$|\nu_\alpha\rangle = \sum_i U^*_{\alpha i} |\nu_i\rangle \tag{7}$$

$$|\nu_i\rangle = \sum_\alpha U_{\alpha i} |\nu_\alpha\rangle \tag{8}$$

where $|\nu_\alpha\rangle$ denotes a neutrino in a definite flavor state, $|\nu_i\rangle$ a neutrino mass state and $U_{\alpha i}$ the corresponding matrix element. The transition matrix U is referred to as the PMNS matrix after Pontecorvo, Maki, Nakagawa and Sakata and can be parameterized as follows:

$$\begin{aligned}&\begin{bmatrix}1 & 0 & 0\\ 0 & c_{23} & s_{23}\\ 0 & -s_{23} & c_{23}\end{bmatrix} \times \begin{bmatrix}c_{13} & 0 & s_{13}e^{-i\delta_{CP}}\\ 0 & 1 & 0\\ -s_{13}e^{i\delta_{CP}} & 0 & c_{13}\end{bmatrix} \times \begin{bmatrix}c_{12} & s_{12} & 0\\ -s_{12} & c_{12} & 0\\ 0 & 0 & 1\end{bmatrix}\\ &= \begin{bmatrix}c_{12}c_{13} & s_{12}c_{13} & s_{13}e^{-i\delta_{CP}}\\ -s_{12}c_{23} - c_{12}s_{23}s_{13}e^{i\delta_{CP}} & c_{12}c_{23} - s_{12}s_{23}s_{13}e^{i\delta_{CP}} & s_{23}c_{13}\\ s_{12}s_{23} - c_{12}c_{23}s_{13}e^{i\delta_{CP}} & -c_{12}s_{23} - s_{12}c_{23}s_{13}e^{i\delta_{CP}} & c_{23}c_{13}\end{bmatrix}\end{aligned} \tag{9}$$

where c_{ij} denotes the cosine of the mixing angle θ_{ij} between the mass eigenstates i and j, s_{ij} denotes the sine of θ_{ij} and δ_{CP} the CP violating phase. CP violation in the neutrino sector has not yet been observed. Current best estimates of θ_{ij} from global fits have a precision better than 15 % with θ_{23} having the largest uncertainty. The current best values are summarized in reference [32].

A neutrino evolves in time by the wave function of the mass eigenstates:

$$|\nu_\alpha(t)\rangle = \sum_i U_{\alpha i} \exp^{-iE_{\nu_i}t/\hbar} |\nu_i\rangle \quad . \tag{10}$$

In a two flavor scenario the probability of finding back an electron neutrino after a given time t is [37]:

$$P_{\nu_e \to \nu_e}(t) = \langle \nu_e|\nu_e\rangle = |U_{e1}|^2 + |U_{e2}|^2 + 2|U_{e1}||U_{e2}|\cos\left(\frac{(m_{\nu_1}^2 - m_{\nu_2}^2)c^4}{\hbar p c^2} ct\right) \quad . \tag{11}$$

As can be seen from Eq. 11, the oscillation probability is proportional to the mass square difference $\Delta m_{21}^2 = (m_{\nu_1}^2 - m_{\nu_2}^2)$. As a consequence, only mass differences can be determined by observing neutrino oscillations. The distance traversed during one period is called oscillation length L and amounts to:

$$L = 2\pi \frac{\hbar p}{\Delta m_{21}^2 c^2} \quad . \tag{12}$$

The current estimates of the matrix elements of the PMNS matrix and the CKM matrix are shown in Fig. 4. As can be seen from Fig. 4, the off-diagonal matrix elements are much larger for the PMNS matrix, causing more mixing between the flavor eigenstates compared to the quark sector.

1.2.2 *Neutrino interactions with matter*

Neutrinos interact with matter via gravitation and the weak interaction. Weak interactions are mediated via one of two force carries referred to as W and Z boson. The W boson is electrically charged while the Z boson is electrically

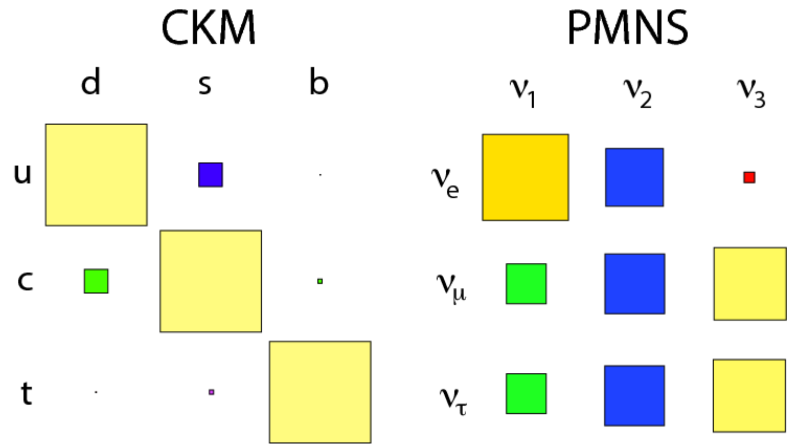

Figure 4: Visual representation of the size of the matrix elements in the two mixing matrices for quark (CKM) and neutrino (PMNS) flavors respectively; the size of the square represents the likeliness of mixing between two states; taken from [38].

neutral. Although the coupling strength of the weak force is comparable to that of the electromagnetic force, the mass of the mediator particles ($M_{W^\pm} \simeq 80\,\text{GeV}$ and $M_Z \simeq 91\,\text{GeV}$) causes the interaction cross sections to be much smaller than that of the electromagnetic force. Hence, the name weak interaction.

Depending on the energy of the neutrino, different interaction modes contribute to the cross section. Below 1 GeV quasi-elastic scattering (QES) dominates; around 1 GeV quasi-resonant scattering (QRS) has a significant contribution; and above 5 GeV deep inelastic scattering (DIS) dominates [39]. The measured cross sections are shown in Fig. 5. The three interaction modes can be differentiated by the state of the nucleus (nucleon) after the interaction. In QES, a single nucleon is kicked out of the nucleus. In QRS, the struck nucleon gets exited (typically Δ-resonance). In DIS, the momentum transfers is so large that the struck nucleon fragments into many particles (mainly light hadrons).

In addition to these different modes, weak interactions can be differentiated in charged current (CC) and neutral current (NC). The exchanged mediator boson is then a $W^\pm$ or Z, respectively. While the NC interaction only transfers momentum and energy, the CC interaction also transfers charge. As a consequence, the neutrino is converted into its corresponding charged lepton. Hence, the outcome of CC interactions differs between neutrino flavors while outcome of the NC interactions does not.

When neutrinos interact with matter they either interact with a nucleon or an electron. With one exception discussed below, the neutrino-nucleon interaction is dominant for all flavors and energies considered in this work.

Measurements of the neutrino-nucleon cross section have been performed since high-luminosity neutrino sources became available and are still performed today [8]. Neutrino beams typically run up to energies of hundreds of GeV. The DIS cross sections can, however, accurately be extrapolated using the precise knowledge of the nucleon structure functions [40]. The main uncertainty in the neutrino-nucleon cross section is then caused by the uncertainties of the parton

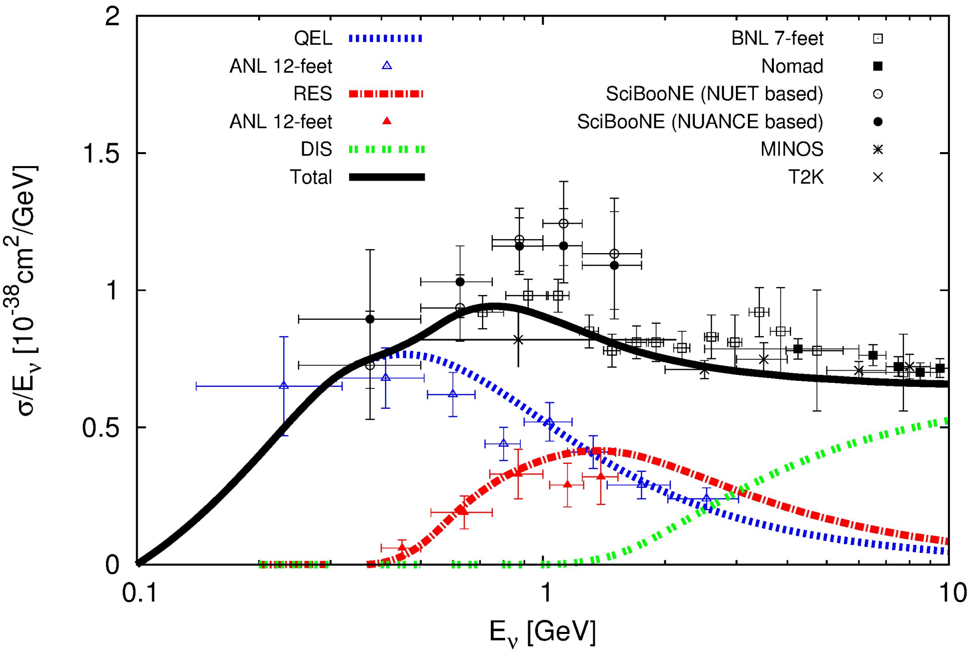

Figure 5: Measured muon neutrino-nucleus cross sections as a function of neutrino energy as taken from [39] (points); the curves correspond to fits of certain models to the data.

distributions. Currently, reliable estimations up to neutrino energies of 10^7 GeV can be made [41]. The resulting neutrino-nucleon cross sections for CC and NC muon neutrino interactions are shown in Fig. 6. As can be seen from Fig. 6, the cross section scales linear with the energy for energies up to 10^3 GeV and is proportional to $E^{0.4}$ at higher energies. This change in dependence is caused by the Z and W boson masses. Neutral current cross sections are about a factor five smaller than the CC cross sections. Anti-neutrino cross-sections are around a factor two lower than those of neutrinos for energies below 100 GeV or so, due to the contribution of valence quarks.

The cross section for a 100 TeV neutrino translates to an interaction length of $250 \times 10^3\,\mathrm{kg\,cm^{-2}}$. For water this equals to a depth of 2.5×10^6 km. Since the average density of Earth is about 5.5 times higher than that of water this translates to an interaction length significantly smaller than Earth's diameter (7.9×10^6 m) thereby making the Earth opaque for high energy neutrinos.

The Earth is not completely opaque for all neutrino flavors. Of the two neutrino interactions, the CC is the one which transforms the neutrino into a charged lepton. The CC interactions of the tau neutrino flavor, discussed in more detail below, produce a tau which rapidly decays into a tau neutrino and other particles. This effect is called "tau regeneration" and allows a certain fraction of tau neutrinos to traverse Earth. Since the cross-section increases with energy and every interaction reduces the energy of the daughter tau neutrino, the energy loss increases with initial neutrino energy. For more details see Chap. 3.1.1.

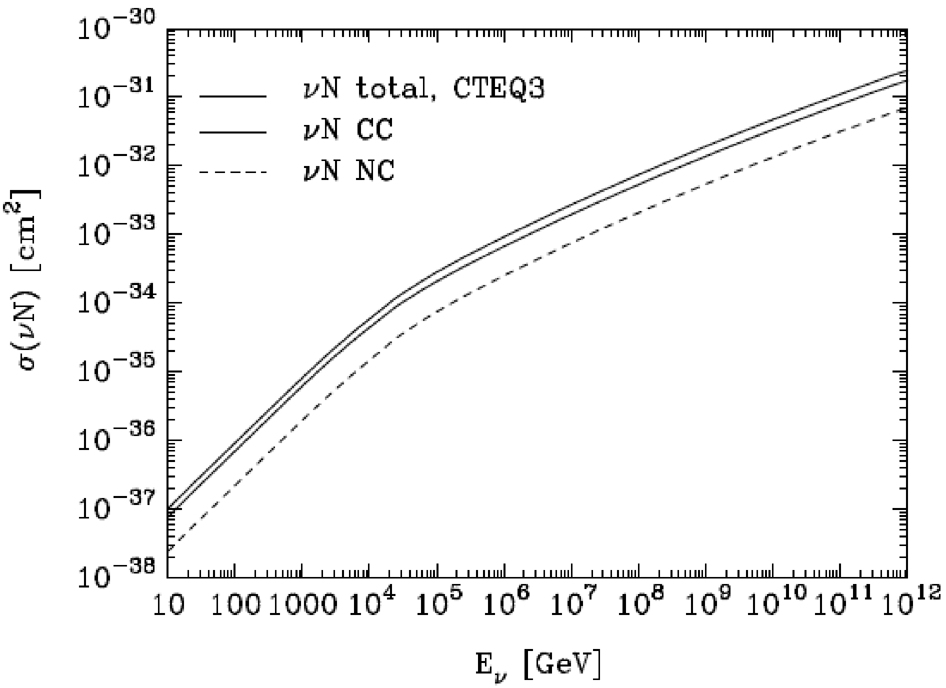

Figure 6: Calculated muon neutrino-nucleon cross section for DIS as taken from [41].

The Glashow Resonance

The neutrino-electron cross section gets much larger for anti-electron neutrinos around an energy of 6.3 PeV [42]. At that energy, the W boson can resonantly be produced: $\bar{\nu}_e + e^- \rightarrow W^-$. The effect was first studied by S. Glashow in 1960 and is consequently named the Glashow resonance.

The shape is well described by a Breit-Wigner function [43] with a width of around PeV. An illustration of the Glashow resonance is shown in Fig. 7. As can be seen from Fig. 7, the neutrino-electron cross sections is about 300 times larger than the neutrino-nucleon cross section at the resonance.

The produced W^- boson has a branching ratio to decay into hadrons of about 68 % and roughly 11 % per flavor to decay into leptons. In the case of an hadronic decay, essentially all energy is deposited in the medium. This mimics a NC interaction in which all energy is transferred to the target. In the case of a leptonic decay, the produced neutrino takes away a substantial amount of energy. This mimics a CC interaction in which some energy is transferred to the target. For example, in the case of the W decaying into an electron, the average deposited energy is 1.57 PeV [43].

Neutrino oscillations in matter: The MSW effect

So far, only neutrino oscillations in vacuum have been considered. Neutrino oscillations are changed when neutrinos propagate through matter, as a direct result of the interactions between neutrinos and matter. The abundance of electrons in normal matter allow for the electron neutrino to interact via CC

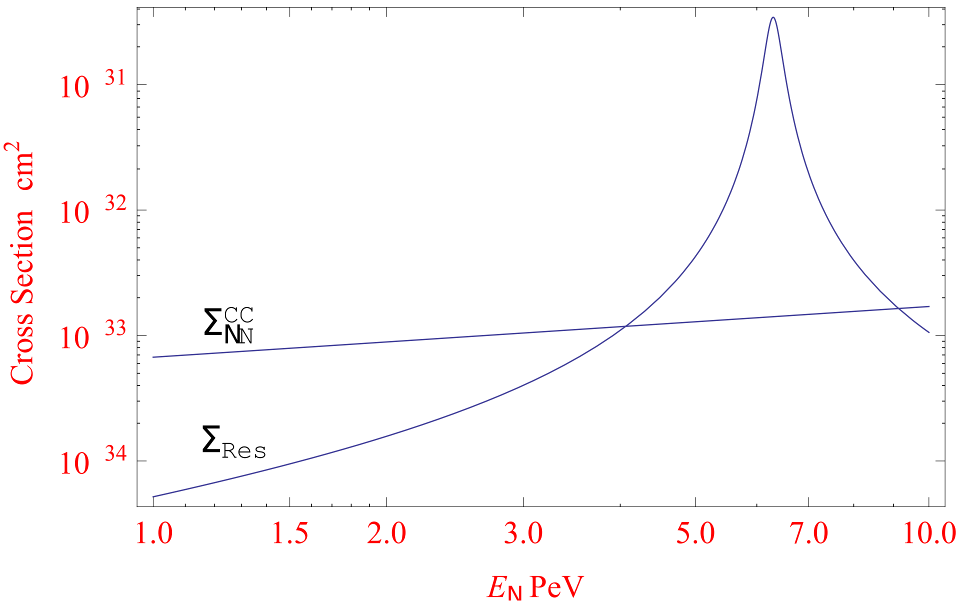

Figure 7: Theoretical predictions of the Glashow resonance cross section (Σ_{res}) and the CC neutrino-nucleon cross section (Σ_{NN}^{CC})as taken from [43].

and NC while maintaining its initial state. This is not the case for muon and tau neutrinos or anti-neutrinos, which can only interact with the electrons via the NC while maintaining the initial state. This assymetry was first pointed out by Mikhaev, Smirnov and Wolfenstein and was subsequently named the MSW effect [44, 45].

In a two flavor neutrino scenario the vacuum oscillation is described by the Hamiltonian:

$$H_V = \frac{\Delta m^2}{4E} \begin{bmatrix} -\cos(2\theta) & \sin(2\theta) \\ \sin(2\theta) & \cos(2\theta) \end{bmatrix} \quad , \tag{13}$$

in analogy with Eq. 9. In matter, the MSW effect gives rise to an additional potential of $V = \pm\sqrt{2}G_F N_e$ where $\pm$ corresponds to neutrino/anti-neutrino, G_F is the Fermi constant and N_e is the electron number density. This potential only effects the electron neutrinos. This causes the Hamiltonian in matter to change to:

$$H_M = \frac{\Delta m^2}{4E} \begin{bmatrix} -\cos(2\theta) + A & \sin(2\theta) \\ \sin(2\theta) & \cos(2\theta) - A \end{bmatrix} \quad , \tag{14}$$

with $A = 2EV/\Delta m^2$. This effectively causes the apparent mixing angle of neutrinos in matter to change [46].

1.2.3 *Neutrino sources*

In this section the different sources and their relevance to neutrino astronomy are summarized. The discussion focuses on the most prominent sources.

Geoneutrinos: The term geoneutrino refers to all neutrinos produced in the Earth. Most of the geoneutrinos are produced in β^- decays of the nuclides ^{40}K,^{232}Th and ^{238}U. These are anti-electron neutrinos with a maximum energy of a few MeV. These neutrinos are not considered in this work.

Reactor neutrinos: Neutrinos generated in nuclear fission reactors are the main source of man made neutrinos. The bulk of reactor neutrinos get produced in the β^- decay of the daughter nucleus resulting from the fission. These are anti-electron neutrinos. Reactor neutrinos have been used to study neutrino oscillations [47] but are not part of this thesis.

Atmospheric neutrinos: Interactions of cosmic rays in the Earth's atmosphere produce mainly charged pions and kaons. Both can decay into charged leptons and neutrinos. Their finite lifetime gives rise to a large flux of neutrinos which is commonly referred to as atmospheric neutrinos. The energy spectrum of the atmospheric neutrino flux is steeper than that of the cosmic rays because the pions and kaons can interact with the atmosphere before they decay. Depending on the energy involved, also muons produced by the decay of pions and kaons can decay before hitting the Earth, thereby producing neutrinos as well.

For initial cosmic ray energies in excess of 1 TeV, the production of charmed mesons becomes significant. These charmed mesons have much shorter lifetimes than pions and kaons. As a consequence, the neutrinos produced in the decays of charmed mesons maintain the cosmic ray energy spectrum to a large extent. Due to the rapid decay of the charmed mesons, these neutrinos are referred to as "prompt neutrinos".

The prompt neutrino flux is poorly constrained by experimental data. To date, the best measurement is performed by IceCube [48]. Although understanding of the prompt flux may be limited, it can safely be assumed that the fraction of tau neutrinos is at least one order of magnitude below that of the other flavors, as charmed mesons heavy enough to decay into tau leptons are produced at a significantly lower rate [49].

The flux of atmospheric muon and electron neutrinos was measured by Antares [50] and IceCube [51, 52]. See Fig. 8 for an overview. For neutrino astronomy, atmospheric neutrinos constitute an important background.

Solar neutrinos: The sun is known to be a powerful source of neutrinos. The model to describe the sun and the processes taking place inside it is called the Standard Solar Model (SSM) [53]. In the SSM, the various reaction chains that fuel the sun and produce neutrinos are included. The main reaction is the fusion of four protons into a helium nucleus. The different processes and their fluxes as a function of energy are shown in Fig. 9. Also, solar neutrinos are not a part of this work.

Cosmic neutrino background: Following Big Bang cosmology, a cosmic neutrino background should be present anywhere in the Universe. These are neutrinos which decoupled from matter about 1 second after the Big Bang [55]. The expansion of the Universe cooled the cosmic neutrino background to a temperature of about 1.95 K (or 16.81×10^{-5} eV). The expected density is about 340 neutrinos per cm^3. The CNB is not part of this work.

Cosmic neutrino sources: Cosmic neutrinos originate somewhere in the cosmos, beyond our solar system. Due to the distinction of cosmic rays into galactic and extra-galactic, cosmic neutrinos are commonly distinguished the same way. To date, no sources of cosmic neutrinos have been discovered with the exception of Supernova SN1987A. Nonetheless, possible galactic sources have

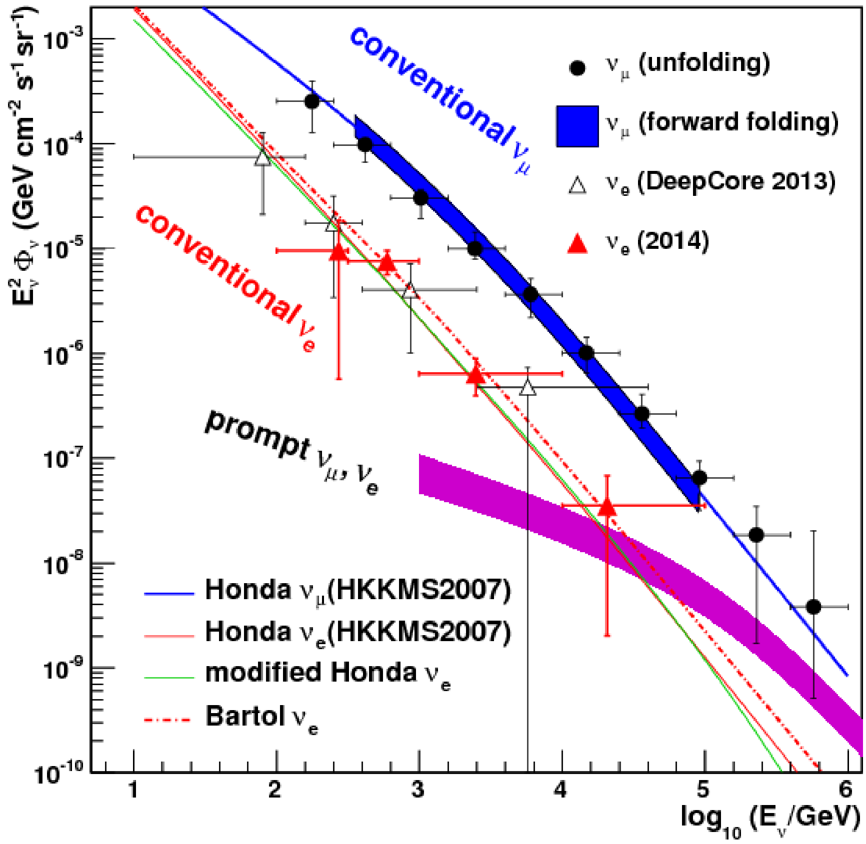

Figure 8: Atmospheric neutrino fluxes as measured by IceCube in [51] together with theoretical calculations.

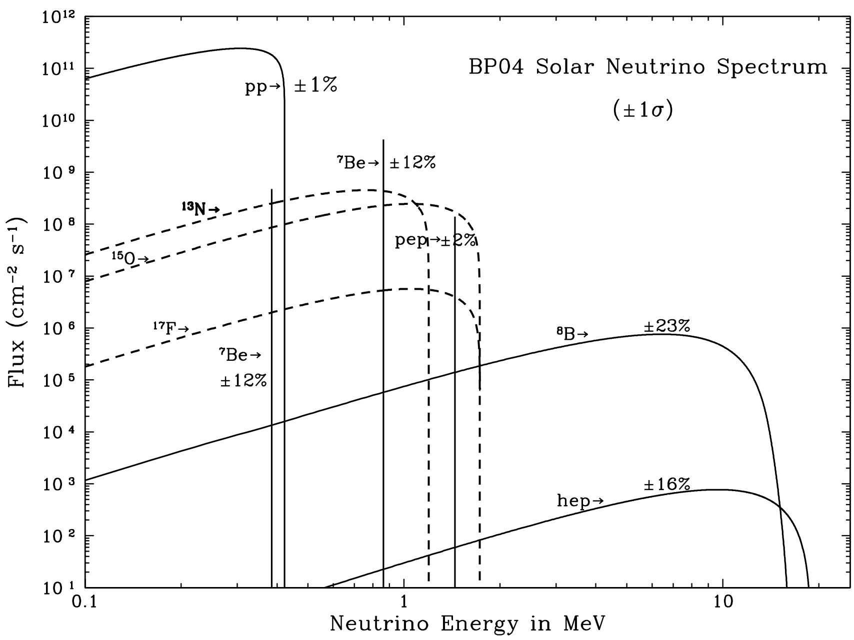

Figure 9: Flux of solar electron-neutrinos as predicted by the BBP04 solar model. Taken from [54].

been identified by gamma ray observations [56]. Based on these observations, three candidate galactic sources have been identified with a neutrino flux large enough to be detected, namely SNRs, RX J1713.7-3946 and RX J0852.0-4622, and one Pulsar Wind Nebula, Vela X. Uncertainties remain regarding the correlation between the observed gamma flux and the assumed neutrino flux of these sources, as different production mechanisms yield different results. Also, extra-galactic sources could produce neutrinos. Since neutrinos are not deflected by magnetic fields, their detection could pinpoint the origin of cosmic rays. The majority of cosmic neutrinos are expected to originate from pion and kaon decays in the vicinity of the source, following the same reasoning as for atmospheric neutrinos. Since the matter density may be lower than that in the Earths atmosphere, the energy spectrum of cosmic neutrinos is generally believed to follow that of cosmic rays.

For all cosmic neutrinos, different scenarios for the flavor composition at the source exist. The standard scenario assuming interactions in analogy to atmospheric neutrinos predict a flavor composition of $\nu_e : \nu_\mu : \nu_\tau = 1 : 2 : 0$ which results from decays of the charged pions, kaons and muons. The two most-important different scenarios are the so-called muon-damped and neutron-beam sources [57]. For the muon-damped scenario it is assumed that the muons from the pion decay loose most of their energy in the matter surrounding the source before they decay. As a result, the daughter neutrinos from these muon decays have such low energies that their flux can safely be neglected. Consequently, the flavor composition at the source is $\nu_e : \nu_\mu : \nu_\tau = 0 : 1 : 0$. For the neutron-beam, it is assumed the neutrinos then are produced from neutron decays leading to flavor composition at the source of $\nu_e : \nu_\mu : \nu_\tau = 1 : 0 : 0$ of purely anti-electron neutrinos. The neutrino flavor ratios at the source translate to a certain flavor ratio at Earth since the neutrinos oscillate during their propagation through the Universe. On average, the three discussed source models roughly oscillate into a flavor ratio at Earth of $\nu_e : \nu_\mu : \nu_\tau \simeq 1 : 1 : 1$. Using a full flavor oscillations calculation (assuming inverted mass hierarchy [58]), the different source flavor compositions translate to different compositions on Earth: $1 : 2 : 0 \rightarrow 0.93 : 1.05 : 1.02$ (pion-decay), $0 : 1 : 0 \rightarrow 0.19 : 0.43 : 0.38$ (muon-damped) and $1 : 0 : 0 \rightarrow 0.55 : 0.19 : 0.26$ (neutron-decay) [59]. It should be noted, that although no source scenario initially produces tau neutrinos, due to the neutrino oscillations, tau neutrinos are expected at Earth for any source composition.

In addition to the flavor composition, cosmic neutrinos also have a mixture of neutrinos and anti-neutrinos. A mechanism for an asymmetric mixture is the imbalance between matter and anti-matter present in the Universe and in the composition of cosmic rays. For a specific model, the resulting flavor compositions for neutrinos and anti-neutrinos at Earth are: 14:11:11 for neutrinos and 4:7:7 for anti-neutrinos [60].

1.2.4 *Neutrino telescopes*

The detection technique employed by cosmic neutrino telescopes to date was proposed by Moisey Markov in 1960 [61]: He suggested to detect Cherenkov radiation from the products of a neutrino interaction (see Sec. 1.2.4.1) in a suitable medium. As these reactions can produce large signatures, cosmic neutrino telescopes instrument up to cubic kilometers of a medium. Neutrino telescopes are usually located deep under ground (or water), in order to shield them from the background of atmospheric muons produced above the telescope. For the detection of the Cherenkov photons photomultiplier tubes are used (see Sec. 2.3).

The first experiment following this approach was the DUMAND experiment off the coast of Hawaii. Due to technical difficulties the project was cancelled in 1995 [62]. Following a series of pioneering projects, the world wide efforts now concentrate in the IceCube project at the South Pole [63], the GVD project in lake Baikal [64, 65] and the Antares [66] and KM3NeT [67] projects in the Mediterranean Sea.

These projects are united in a umbrella organization called the Global Neutrino Network (GNN) [68]. The GNN aims at combining the efforts of all neutrino telescopes in order to devlop a coherent strategy and promote an exchange of ideas among them.

Since this work is made for the KM3NeT experiment, in the following the most important aspects of detecting neutrino interactions in water are discussed.

1.2.4.1 *Cherenkov Radiation*

Cherenkov radiation is named after the Russian scientist Pavel Cherenkov who was the first to study the process in 1933 [69]. Together with theoreticians Il'Ja Frank and Igor Tamm, Cherenkov was awarded the Nobel Prize in 1958 [70]. Cherenkov radiation occurs when a charged particle moves through a transparent medium with a speed exceeding the speed of light in that medium. This causes the medium to be asymmetrically polarized with respect to the particle trajectory which gives rise to a changing dipole moment causing the radiation. Properties of the Cherenkov radiation such as the speed threshold and the radiation angle are governed by the refractive index of the medium. The phase velocity of light v in a medium is given by:

$$v = c/n \quad , \tag{15}$$

where c is the speed of light in vacuum and n the refractive index of the medium. The angle of the emitted light with respect to the charged particle trajectory is given by:

$$\cos\theta_C = \frac{1}{n\beta} \quad ,$$

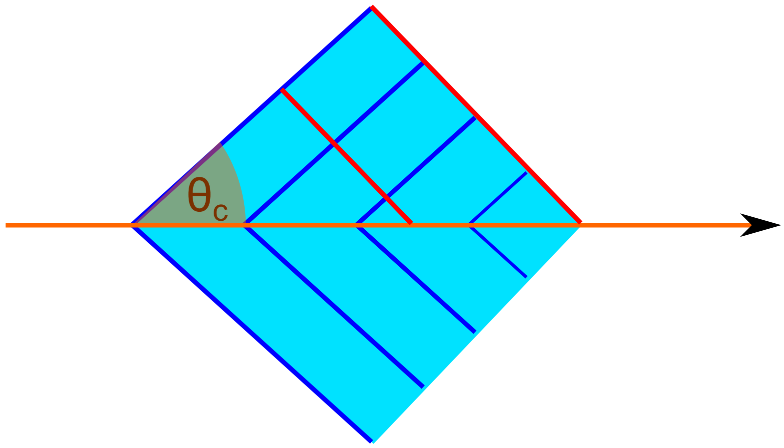

Figure 10: A sketch of a charged particle (orange line) traversing water. The resulting Cherenkov cone emitted at θ_C; the dark blue lines indicate single photon trajectories and the red lines indicate the surface crossed by these photons at equal times.

where θ_c is the angle of emittance and β the speed of the charged particle (relative to the speed of light in vacuum). The frequency spectrum is described by the Frank-Tamm formula [71]:

$$\frac{d^2E}{d\omega dx} = \frac{q^2}{4\pi}\mu(\omega)\omega\left(1 - \frac{c^2}{v_p^2 n^2(\omega)}\right) \quad ,$$

where ω is the frequency, q is the electric charge of the particle, $\mu(\omega)$ and $n(\omega)$ are the frequency dependent permeability and index of refraction of the medium. The number of emitted photons per unit track length x and wavelength λ are given by:

$$\frac{d^2N}{d\lambda dx} = \frac{2\pi q^2}{\lambda^2}\alpha \sin^2(\theta_C) \quad ,$$

where $\alpha = {}^{2\pi e^2}/_{hc}$ and e is the unit electric charge.

For typical conditions found in the abyss of the Mediterranean Sea this results in a Cherenkov angle of $\theta_C = 42.2°$ and a wavelength range from 350 nm to 550 nm. A sketch of a charged particle traveling through water and the resulting Cherenkov cone is depicted in Fig. 10.

1.2.4.2 *Light propagation in water*

While the photon phase velocity determines the Cherenkov angle, the photons actually propagates at a speed equal to the group velocity. The refraction indices of group and phase velocity n and n_g both depend on the wavelength. The values for KM3NeT are shown in Fig. 11.

While propagating through water, light will undergo scattering and absorption. Scattering describes the process of a photon changing its direction whereas absorption describes the disappearance of a photon. Both effects depend on the

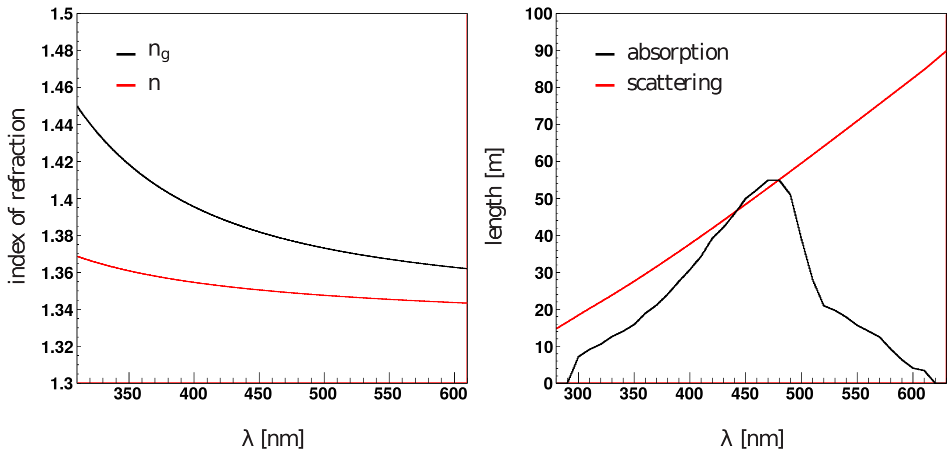

Figure 11: Indices of refraction (left), absorption length (right) and scattering length (right) as a function of the wavelength of the light for KM3NeT water taken from [72].

wavelength of the light. The probability for such a process to happen can be expressed in form of a length. The typical scattering and absorption lengths of KM3NeT are shown in Fig. 11.

In the deep waters of the Mediterranean Sea, the light scattering is very forward peaked. The average cosine of the scattering angle is around $\cos(\theta_c) = 0.9$. For KM3NeT, recent simulations indicate that direct and single scattered light constitute the dominant signal [73].

1.2.4.3 *Detection Signatures*

The different neutrino flavors in combination with the different weak interaction modes lead to distinct signatures in the detector. All neutrino interactions are a combination of two signatures, namely: shower and track. In the following, first the shower and track signatures are discussed. This is followed by a description of the NC and CC interactions in terms of combinations of track and shower signatures.

Track Signature

A track signature corresponds to a single charged particle that traverses the medium producing Cherenkov light on its way. At the energies under consideration, the only particle with a sufficiently long lifetime and mean free path are muons. Therefore, the track signature usually refers to CC interactions of muon neutrinos. Muons with an energy of a TeV or higher have their lifetime significantly prolonged to travel for kilometers through water at the speed of light. During their flight, muons can loose energy due to Bremsstrahlung and other processes. Most of these processes will also lead to the production of Cherenkov light thereby contributing to the detectable signal. Due to momentum conservation, these photons are emitted at an angle close to the Cherenkov angle with respect to the muon direction. The total signal of a muon is therefore primarily observed at the Cherenkov angle with respect to its path with contributions at different angles.

Shower Signature

A shower signature corresponds to a multitude of charged particles which each produce Cherenkov light. A particle shower can be caused by an initial particle which via a decay or interaction produces other particles. In this process, energy is converted to mass. The particles produced can subsequently decay or interact, thereby producing even more particles. This avalanche comes to a halt once the energy of the particles is too low to produce new particles. The typical length of a shower is governed by the energy and type of the initial particle. The logarithm of the initial energy correlates with the number of steps, due to the iterative nature of the process. The typical length of each interaction step is governed by the different mean free paths of the particles.

One important characteristic of a shower is the shower maximum, which is defined as the point in the shower evolution where the largest amount of particles exist. For an initial electron, the position of the shower maximum and light emission profile for a given initial energy is shown in Fig. 12 [74]. The distribution for hadronic showers is similar, but typically 1 m shorter. This can be explained by the larger average mass of hadrons compared to that of an electron and the difference in interaction length. At a given energy, the amount of photons produced by a hadronic shower is typically 80 % of the amount of light produced by an electromagnetic shower. While the length and total amount of photons may be different, the emission profiles are very similar.

The distribution of emission angles for showers is well described by the distribution shown in Fig. 13 independent of the shower energy [75]. The figure shows a broad distribution of emission angles, which can be attributed to the spread in directions of the particles. Due to momentum conservation, a majority of photons is still emitted at the Cherenkov angle.

Neutral Current Interaction Signatures

In a NC interaction, a Z boson is exchanged between the neutrino and a nucleon. In the process, the neutrino transfers momentum and energy to the nucleon and continues thereafter. In the absence of interference terms, the NC interaction does not distinguish between neutrino flavors. At energies of interest, the interaction causes the nucleon to fragment (DIS), resulting in a hadronic shower. A diagram of the NC interaction is shown in Fig. 14a.

Charged Current Interaction Signatures

In a CC interaction a $W^{\pm}$ boson is exchanged between the neutrino and the nucleon. Since the W boson is electrically charged, the conservation of charge and lepton number causes the neutrino to transform into its corresponding charged lepton. This causes the detector signatures of the electron, muon and tau neutrinos to differ. As for the NC interaction, the nucleon with which

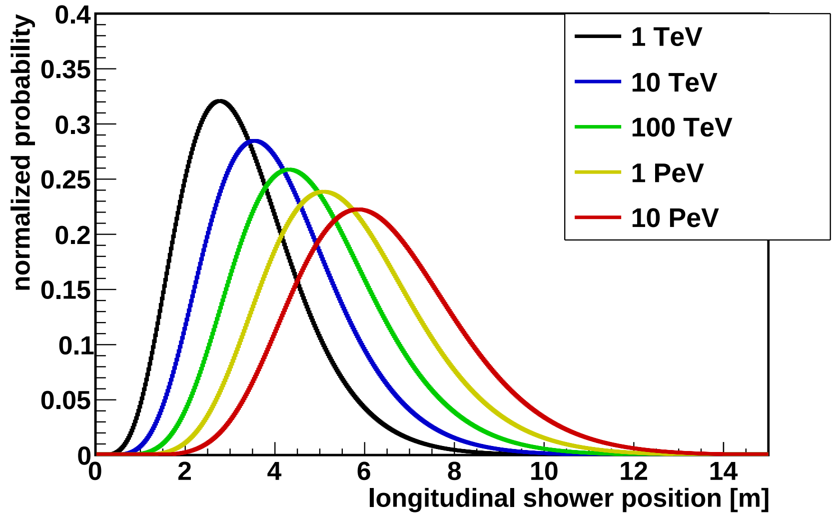

Figure 12: Longitudinal electromagnetic shower emission profiles for different initial electron energies; the shower maximum corresponds to the point with the maximal probability.

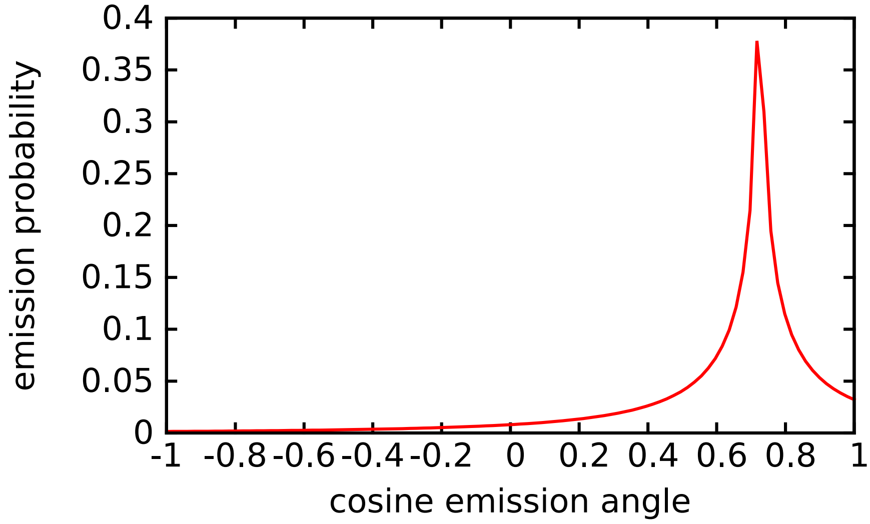

Figure 13: Photon angular emission profile independent of shower energy.

the neutrino interacts gets fragmented, producing a hadronic shower at the interaction vertex.

Electron neutrino: Electrons have a short mean free path length in water, which leads to an electromagnetic shower. As a result, the hadronic and electromagnetic shower overlap. Therefore, electron neutrino CC interactions have a signature of a single shower event similar to NC interactions. See Fig. 14b for a diagram.

Muon neutrino: Muons have a much longer mean free path compared to electrons due to their larger mass ($\approx 200 \times m_e$), which suppresses electromagnetic interactions with the medium. This leads to a signature with a hadronic shower and a track. See Fig. 14c for a diagram.

Tau neutrino: Taus have an even larger mean free path due to their immense mass ($\approx 9 \times m_\mu$). However, their lifetime of 290.6×10^{-15} s is seven orders of magnitude smaller than the muon lifetime, causing them to rapidly decay. Only at high energies the tau lepton can travel visible distances thanks to relativistic time dilation (at $E_\tau = 1$ PeV the tau mean lifetime corresponds to a flight length of about 50 m). Tau neutrino CC interactions can lead to different signatures due to the various tau lepton decay modes: In 17.4 % of the cases the tau decays into a muon which appears as a track. This interaction is called the "Sugar Daddy" signature, see Fig. 14e for a diagram. The remaining tau decay modes (83.6 %) cause either an electromagnetic or hadronic shower at the tau decay position. These events have therefore two showers: the hadronic shower at the neutrino interaction vertex and a second shower at the tau decay position. Different from the electron neutrino interaction, these can be separated by visible distances. Therefore, the double shower nature gives rise to the name of "Double Bang" events. See Fig. 14d for a diagram.

Neutrino flavor identification in a neutrino telescope

Identifying the neutrino flavor of a detected interaction with a neutrino telescope opens up new measurements opportunities and enhances background suppression. Currently, neutrino telescopes categorize events in two classes: tracks and showers. This does not yield an actual flavor reconstruction because NC interactions are classified as shower events for all flavors and tau CC interactions can fall into either category.

Certain CC interactions allow for a flavor identification. For example, the "Double Bang" interaction for tau flavors is unambiguous, allowing for a clean tau flavor identification. As stated earlier, tau neutrinos have low atmospheric backgrounds compared to the other flavors. An ideal full three flavor identification allows to determine the flavor composition at the source of cosmic neutrinos.

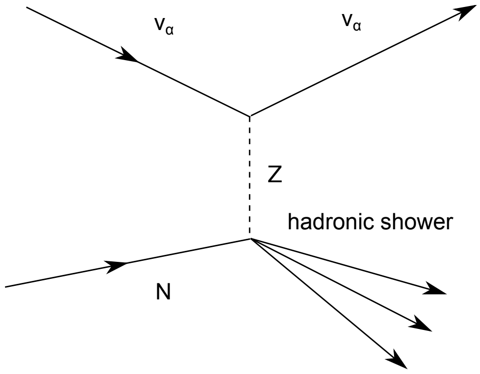

(a) Neutral current interaction for all three neutrino flavors.

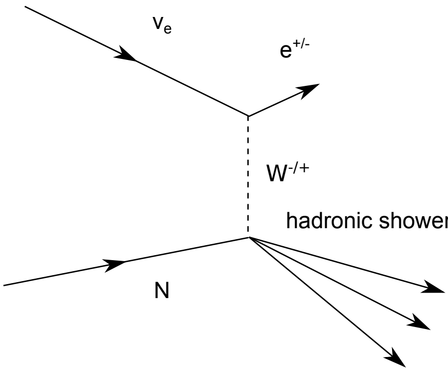

(b) Charged current interaction for electron neutrinos causing a electromagnetic shower.

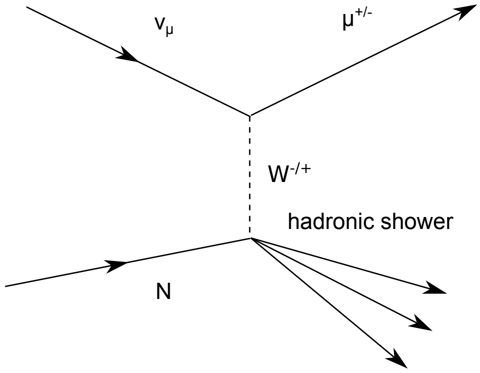

(c) Charged current interaction for muon neutrinos lead to a muon track.

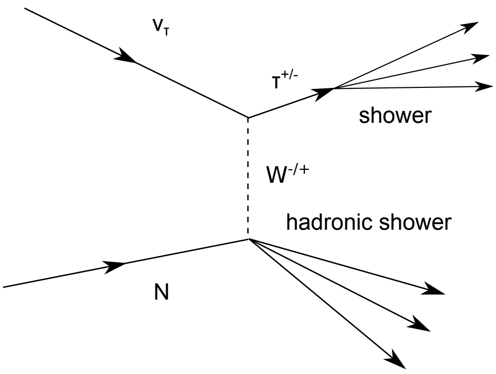

(d) Charged current interaction for tau neutrinos with the tau decaying to an electron or hadrons leading to a second shower.

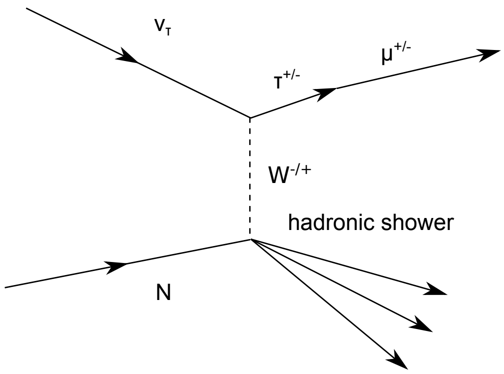

(e) Charged current interaction for tau neutrinos with the tau decaying to a muon (neutrinos neglected).

Figure 14: Diagrams for the different neutrino interactions in water; no distinguishment made between neutrino and anti-neutrino (all denoted ν).

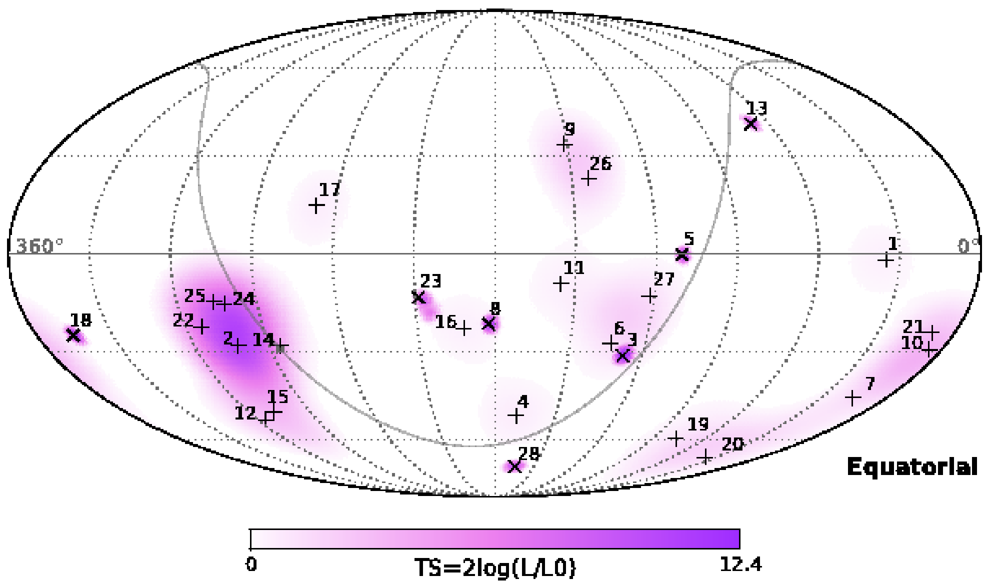

Figure 15: Skymaps of IceCube flux neutrinos; Vertical crosses (+) denote shower-like events and angled crosses (x) denote track-like events; As measured in 2013 [80].

1.2.5 *Cosmic neutrino observations: SN1987 and the IceCube flux*

So far, two observations of neutrinos of cosmic origins have been made, namely supernova SN1987A and the excess of high energetic neutrinos by IceCube in 2013.

In 1987 the star Sanduleak in the Large Magellanic Cloud core-collapsed into a supernova. The supernova was around 51 kpc away and visible by the naked eye. It was the closest observed supernova since 1604 and therefore the first opportunity for modern astronomy to study a supernova in detail. About a decade before SN1987A, the first large neutrino detectors Kamiokande-II and IMB were put into operation. Together these experiments detected 20 neutrino interactions within 13 s of SN1987 [76, 77]. These observations allowed further insights into the mechanisms of core-collapses and neutrino related alternative theories [78].

In November 2013 the IceCube collaboration announced the detection of two neutrino interactions of around 1 PeV energies [79]. Within the same year a follow up analysis of a two year data set yielded another 26 events between 30 TeV to 1200 TeV [80]. Together, these 28 neutrinos were inferred to be of cosmic origin as they were with 4σ significance incompatible with the atmospheric background. Of these initial 28 neutrino events, 21 are shower-like and 7 track-like events. The events are shown in Fig. 15. Today, no point-source(s) could be identified, possibly due to the poor angular resolution for shower events.

The latest results include an all sky search performed for so-called high energy starting events (HESE). These events are required to have their neutrino vertex in the inner part of the detector volume and to have a deposited energy of at least 60 TeV in that volume. By limiting the volume to an inner part, the outer edge of the detector can be used for suppressing the atmospheric background, hence making an all sky search possible. The selection leaves 32 events in 4 years of IceCube data of which 8 are track-like and the rest shower-like, with 22 from the southern sky (4 tracks). The current best flavor fit of the IceCube results are in agreement with a $\nu_e : \nu_\mu : \nu_\tau$ flavor ratio of $1:1:1$. Due to low statistics and the lack of a powerful tau neutrino identification, the flavor ratio fits are still unprecise.

The present observations do not yield in a definite result for the cosmic neutrino flux. Corresponding to the cosmic ray flux, the neutrino flux can be described by a normalization Φ and a spectral index Γ. The results of the different analysis assuming a constant spectral index and no cut-off are summarized in Fig. 16. The fit results prefer a scenario with a cut-off at 3 PeV. Also other groups analyzed the IceCube data considering various spectral indices and cut-off scenarios but no clear answer could be found [60].

For the found spectral indices between $\Gamma = 2$–2.8 the lack of signals from the Glashow resonance indicates that the spectrum either has an energy cut-off somewhere between 3 PeV and 4 PeV, an asymmetry between electron and anti-electron neutrino flavors or a changing spectral index.

The presence of such a cut-off energy is in conflict with the absence of such a cut-off in the cosmic ray spectrum. This tension could be mended, as a recent analysis by IceCube indicates a 1.1σ difference between North-South directions compared to an isotropic flux [59]. Thereby indicating a possibly larger galactic flux component than assumed. Since for the galactic component, a cut-off at these energies is not so unlikely. Future measurements will help to scrutinize this possible asymmetry.

An asymmetry between the flux of electron and anti-electron neutrinos could be explained by certain cosmic ray interactions such as proton-photon interactions. The low statistics of PeV neutrinos make it currently impossible to reliably quantify such an asymmetry. While some sources may have a suitable mechanism to produce such an asymmetry it is not clear why this should be the case for all sources [60].

A change in spectral index ("broken power law") allows for a softer spectrum for neutrino energies above 3 PeV, thereby effectively reducing the flux of neutrinos present at the Glashow resonance. Currently, non of the performed fits to the IceCube data significantly improve using various broken power laws. Consequently, the data does not indicate the broken power law scenario to be more probable than a single power law [60].

Of the three discussed scenarios, the existence of a cut-off energy in the spectrum seems to be most likely, as it slightly improves fit results.

In summary, there is a strong case for another large scale neutrino telescope. The KM3NeT experiment will measure the IceCube flux with a different methodology, improved resolutions and complementary field of view.

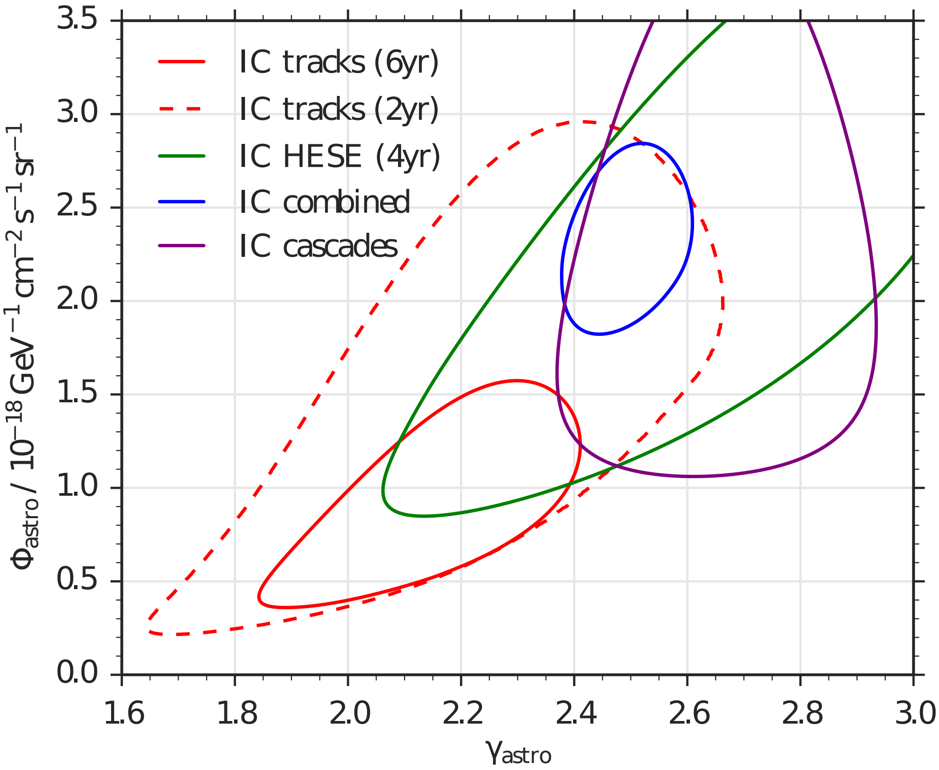

Figure 16: Results of different IceCube analysis measuring the astrophysical flux parameters Φ and Γ taken from [81]; lines show the 90 % confidence areas intervals; γ_{astro} refers to the spectral index Γ and label cascades to shower signatures (see text).